International Journal of Technology (2017) 4: 737-746
ISSN 2086-9614

MEASURING THE EFFECT OF STRENGTHENED CONCRETE ON THE FRACTURE CHARACTERISTICS OF NOTCHED CONCRETE BEAMS THROUGH A THREE-POINT BEAM TEST

Atur P.N. Siregar[1*]

[1]*Department of Civil Engineering, Faculty of Engineering, Tadulako University, Jl. Soekarno Hatta Km. 9, Palu, 94118 Sulawesi Tengah, Indonesia*

(Received: August 2016 / Revised: May 2017 / Accepted: July 2017)

ABSTRACT

This study explores the effect of increased concrete strength on the behavior of concrete failure. Experimental testing using a three-point bend (TPB) test proposed by RILEM was carried out to calculate the value of fracture energy *(G_F)*, stress intensity factor *(K_{IC})*, and characteristic length *(lch)* of the concrete. The values of G_F and l_{ch}, which are proportional to the fracture process zone based on the fictitious crack model, were employed to determine the effect of concrete strength on the concrete's fracture characteristic. K_{IC} was engaged to describe the initial crack in the concrete. Four different concrete strengths of 40, 47, 53, and 100 MPa—were manufactured to produce notched beam specimens with single-sized notches 25 mm deep. Results revealed that the values of G_F and K_{IC} increased in the stronger concretes. However, the value of l_{ch} decreased significantly as concrete strength increased.

Keywords: Characteristic length; Concrete strength; Fracture energy; Stress intensity factor

1. INTRODUCTION

Concrete is a composite material used widely in the construction industry. The superior performance of increasing concrete strength has attracted engineers to incorporate it into the design of modern high-rise buildings, long-span bridges, towers, and other such structures. Though these designers use the product because of its strength, they often fail to consider the concrete's fracture characteristics. This can lead to catastrophes such as the Hanshin viaduct in Kobe, Japan; the Cypress viaduct in Oakland, California; the Malpasset arch dam in the French Maritime Alps, the Schoharie Creek bridge in New York, and a Norwegian oil platform, indicating that such structure failures are due to the absence of concrete fracture characteristic assessment (Bazant & Becq-Giraudon, 2002). Those notable structures failure events should alert engineers that structural integrity depends greatly on the behavior of the materials used in construction, and as such every characteristic of the concrete influenced by constituent materials must be considered carefully during structural design to ensure the resiliency of reinforced high strength concrete structures.

Ince and Alyamac (2008) investigated a fracture parameter—critical crack opening displacement (CTOD)—as a function of the water cement (w/c) ratio. The experimental results indicated that CTOD fell as the w/c ratio decreased. Similarly, Prokopski and Langier (2000) demonstrated that the critical stress intensity factor *(K_{IC})* of concrete correlated with the w/c ratio in that an increased amount of water in the concrete mix (high w/c) caused K_{IC} to drop

*Corresponding author's email: atur_pns@yahoo.com, Tel. +62-451-454014, Fax. +62-451-454014
Permalink/DOI: https://doi.org/10.14716/ijtech.v8i4.9486

significantly. W/c ratio is a key factor in producing a stronger bond between paste and particles; concrete with a low w/c ratio produces a better interfacial transition zone than that with a high w/c ratio, and the zone influences the fracture process.

The experimental results of Prokopski and Langier (2000) and Ince and Alyamac (2008) showed that the w/c ratio of concrete affected the value of both K_{IC} and CTOD. Despite the known link between w/c ratio and the compressive strength of concrete, experimental studies of concrete strength higher than 55 MPa are lacking. The present study, therefore, will investigate the effect that increasing compressive strength has on the concrete's fracture characteristics in scenarios where the concrete strength is between 40 and 100 MPa.

2. FRACTURE CHARACTERISTICS OF CONCRETE

2.1. Fracture Energy (G_F)

A common property used to describe the fracture characteristic of brittle, composite materials such as concrete is G_F. In the present study, the G_F value for each specimen was calculated using the corresponding load versus the mid-span deflection curve based on the RILEM TC50-FCM recommendation (RILEM, 1985) and the effect of the beam's self weight was considered as follows:

$$G_F = \frac{W_o + mg\delta_o}{(d - a_o)t} \tag{1}$$

where G_F is the total fracture energy; W_o is the area under the load deflection curve; m is the total mass of specimens between the supports; g is gravity; δ_o is the end deflection at P = 0; and d, a_o, and t are the height of the sample, depth of the notch, and width of the sample, respectively. The experimental results of the concrete's G_F values are shown in Table 1.

Table 1 Average value of mechanical and fracture parameters of concrete

f_c (MPa)	E (MPa)	f_t (MPa)	K_{IC} (MPa.$\sqrt{m}$)	G_F (N/m)	l_{ch} (Mm)
40	35000	4.56	20.45	115.1	326
47	38000	5.56	24.63	115.1	326
53	40000	6.38	23.68	115.1	288
100	45000	9.03	41.91	160.0	211

2.2. Critical Stress Intensity Factor (K_{IC})

The K_{IC} parameter indicates the initial crack that occurs in the material. It depends on the applied load, boundary conditions, crack length, and structural geometry of the specimen (Shah et al., 1995). The K_{IC} values of the samples were determined using a three-point bend (TPB) test, which was carried out by adopting the RILEM TC89-FMT recommendation (RILEM, 1985) as follows:

$$K_{IC} = \frac{3(P_c + 0.5W)\left(S(\pi a_c)^{0.5} g\left(\frac{a_c}{d}\right)\right)}{2d^2 t} \tag{2}$$

in which

$$g\left(\frac{a_c}{d}\right) = \frac{1.99 - \left(\frac{a_c}{d}\right)\left(1 - \frac{a_c}{d}\right)\left[2.15 - 3.93\left(\frac{a_c}{d}\right) + 2.70\left(\frac{a_c}{d}\right)^2\right]}{\sqrt{\pi}\left[1 + 2\left(\frac{a_c}{d}\right)\right]\left[1 - \left(\frac{a_c}{d}\right)\right]^{\frac{3}{2}}} \tag{3}$$

where P_c is the critical maximum load, W is the self weight of the beam, S is the span of the specimen, a_c is the critical effective elastic crack length, d is the depth of specimen, and t is the width of specimen. The results of the concrete's K_{IC} values are shown in Table 1.

2.3. Characteristic Length (l_{ch})

Concrete brittleness was investigated using the model proposed by Hillerborg (1976), which calculated the characteristic length of the concrete dependent on modulus elasticity *(E)*, G_F, and tensile strength (f_t) as shown:

$$l_{ch} = \frac{EG_F}{f_t^2} \tag{4}$$

The experimental results regarding the characteristic length of the concrete are shown in Table 1.

3. EXPERIMENTAL SETUP

3.1. Material

Portland cement, a Cement (CEM) Type I material with a specific surface area of 338 m^2/kg, was employed to make all the specimens in this study. Fly ash compliant with BS EN450-1 was used as an additional binder in the mix. The gravel-coarse aggregate and sand used in the concrete mix ranged in size from 16 mm down to 5 mm and from 4 mm down to 0.30 mm, respectively. A modified polycarboxylate-based superplasticizer was engaged to create an adequate workability of 120±20 mm. A concrete mix designed to produce four different concrete strengths was used to manufacture the notched beams shown in Table 2.

Table 2 Concrete mix proportions

Item	f_c' = 36 MPa	f_c' = 45 MPa	f_c' = 53 MPa	f_c' = 95 MPa
	Ratio (kg)	Ratio (kg)	Ratio (kg)	Ratio (kg)
Cement	1	1	1	1
Fly ash	0.20	0.25	0.25	0.25
Microsilica	-	0.03	0.05	0.10
Total water	0.53	0.40	0.31	0.23
dia. 16 mm	1.95	1.31	1.31	1.74
dia. 10 mm	1.00	0.52	0.52	0.54
Sand	2.18	1.91	1.91	2.07
Super-plasticizer	-	-	0.002	0.0042

3.2. Specimen Preparation and TPB Test Setup

Cubes of 100×100×100 mm and prisms of 150×150×300 mm were used to measure the compressive strength and modulus elasticity of concretes following BS EN 12390: Part 3 (2001). Beam specimens 100 mm wide, 100 mm deep, and 500 mm long were used for the TPB test as shown in Table 3, along with a number of samples for corresponding compressive strengths. The water cured method was applied to all specimens for 28 days before testing. Notches with a depth of 25 mm (a_o) were created using a rotary cutter with a 2.5 mm-wide blade. (The arrangement of the TPB test setup is shown in Figure 1.) A servo-hydraulic, closed-loop testing machine in the Material and Concrete Laboratory at the University of Surrey, UK was used to conduct the TPB test, as shown in Figure 2.

4. RESULTS AND DISCUSSION

Per the Comite Euro-International Du Beton (CEB-FIP) report on high strength concrete (HSC) (Shah & Ahmad, 1994), a concrete may be considered an HSC if it has a minimum 28-day compressive strength of 60 MPa. The findings of the present study indicate that concrete with a compressive strength of 100 MPa may be classified as an HSC. Concretes with compressive strengths of less than 60 MPa (i.e., 40, 47, and 53), are defined as normal strength concretes (NSCs).

Table 3 Dimension of notched beam specimens

Beam	Number of samples	D (mm)	L (mm)	S (mm)	a_o (mm)	t (mm)
f_c' = 40 MPa	7	100	500	300	25	100
f_c' = 47 MPa	7	100	500	300	25	100
f_c' = 53 MPa	7	100	500	300	25	100
f_c' = 100 MPa	7	100	500	300	25	100

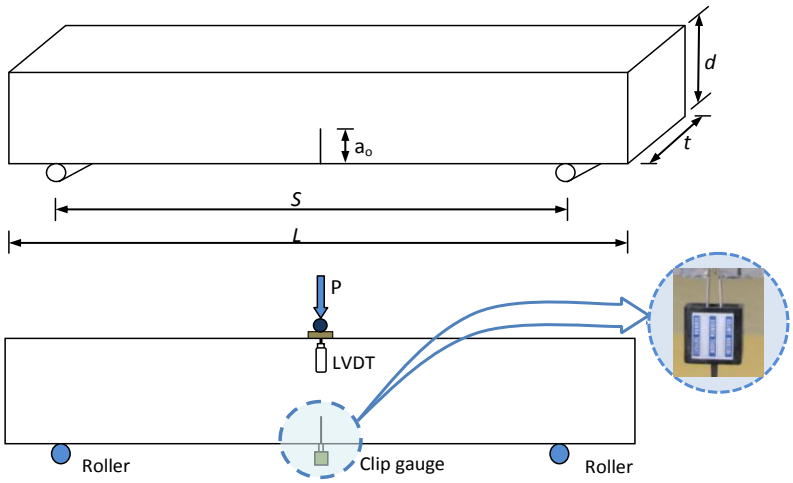

Figure 1 Geometry of specimen and test setup showing detail of clip gauge attachment

Figures 3 and 4 show the responses of specimens manufactured with various concrete strengths to a point load on the notched beam. Stress was calculated as the flexural strength of the concrete using $f_t = M.y/I$ with $M = PS/4$ for the three-point bending. These calculations did not include the beam's self weight because the difference in actual stress was less than 0.5%; y was half the ligament height (mm), I the moment inertia of the ligament (mm^4), P the applied load (N), and S the support length (mm). Concrete strain was measured at the tip of the notch.

Figure 3 shows the variability of the experimental results for the different concrete strengths. The tendency towards variability in the experimental results increased as concrete strength increased. Although these results were gathered from only seven samples, a trend of softening NSC and HSC curves were observed, as shown in Figure 4. The slope of the softening curve of concrete with a compressive strength of 100 MPa (HSC) declined at a much steeper rate than those with compression strengths of 40, 47, and 53 MPa (NSC).

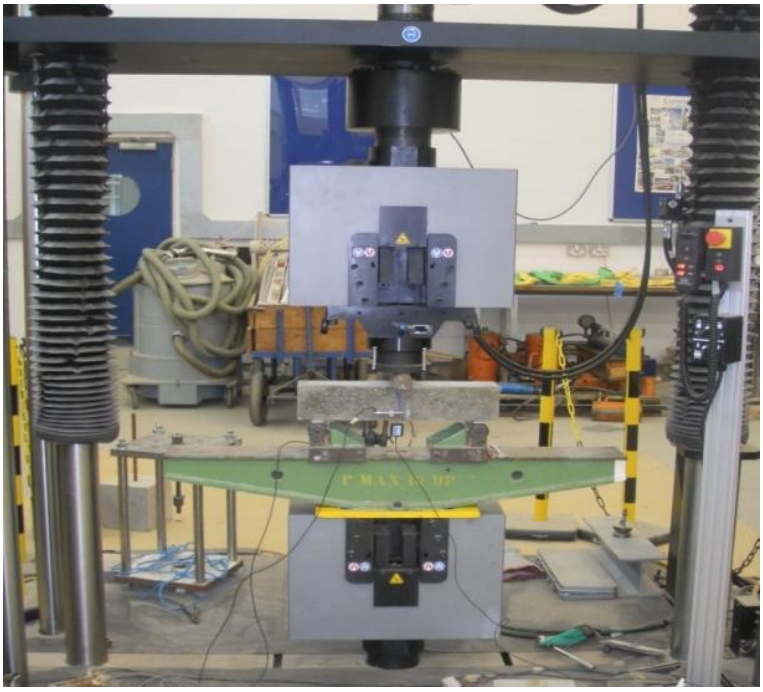

Figure 2 Servo-hydraulic closed-loop testing machine

Peak stress, which represents concrete f_t, depended on the strength of the constituent materials used in forming the concrete. Because the strength of the bulk paste matrix, aggregate/cement interface zone, and aggregate were sufficient to resist applied stress, the linear part of the stress–strain curve increased proprotionally in the present study until a microcrack occured in the concrete. This microcrack created a non-linear part of the stress–strain curve. The presence of voids in the concrete (i.e., defects) as a result of the reaction between cement and water induced the distribution of applied stress in the concrete. The applied stress then concentrated at the edges of the voids (Picard, 2006). As a result of this mechanism, paticles debonded from the matrix in the concrete's bulk paste matrix and cement/aggregate interface zone. This demonstrates that high voids require low tensile stress, as shown by the NSC specimens (see Figure 4).

In material with fewer defects or fewer voids in the concrete (i.e., low porosity), a high tensile stress was required to break the material. HSC was observed to have low porosity yields and higher peak stress than NSC. However, the softening curve of HSC declined much more sharply than that of NSC. At or just before peak stress, inelastic zones appeared and reflected back to the fracture process zone. The pre-excisting microcrack started to grow, and new microcracks began due to debonding between particles and the matrix. The propagation of intial cracks deflected when they reached the aggregate particle. Increasing the applied load caused a coalescence of microcraks, culminating in a single macrocrack. Propagation of the macrocrack reflecting the development of the fracture process zone affected the softening behavior of the stress–strain curve. The normal tensile stress increased gradually from the initial open crack tip, then reached the f_t of the material at the end of the facture process zone. Propagation of the intial open crack tip was resisted by cohesive stress within the fracture process zone due to interlocking particles (Scholtès, 2013), offering additional fracture resistance. This cohesive stress is present in the elastoplastic of brittle material (Scholtès, 2013) such as concrete. The stress-transferring capacity in the softening zone was observed to depend on the sliding friction between the crack surface (Wittmann, 2002), which exists owing to the interlocking of two crack surfaces (aggregates are pulled from the matrix), and aggregate stiffness. It is

hypothesized that the contribution of interlocking surfaces and the sliding friction to the G_F in NCS increased when crack surfaces were more tortuous and the tail-softening curve longer. In HSC, aggregate and paste-matrix stiffness, which control the crack surface equally, tended to fail on both sides, resulting in a straight crack line (see Figure 5) and a steep tail-softening curve (see Figure 4).

Regarding tensile ruptures in NSCs with compressive strengths up to 30 MPa, cracks only occurred in the matrix or along the cement/aggregate interface zone (Sagar, 2013). The present experimental results revealed that the softening curve for concrete with a compressive strength up to 53 MPa (NSC) had a similar kick point (see Figure 4), where the curve turned over considerably and ended up with a higher tail. Similar results regarding tensile rupture in the cement/aggregate interface zone were observed in the current study in concrete with a compressive strength of up to 53 MPa. However, the variation of paste matrix stiffness due to concrete strength influenced the amount of load-carrying capacity. Still, the HSC behaved differently than the NSC. Although the kick point of the HCS was farther than that of the NSC, the intial slope of the softening curve was much steeper and the end tail of the softening curve closer to the normal concrete curve (see Figure 4). In the HSC, applied stress was distributed properly to the particles in the concrete due to the lack of porosity and better paste matrix, and thus cracks propagated in the passing cement/aggregate interface zone and through aggregate particles (see Figure 5). In this case, the stiffness of the paste matrix in the vicinity of the aggregate dictitated the level of crack propagation. As shown in Figure 4, the decline of the end tail softening curve (after the second kick point) was similiar to that of the NSC.

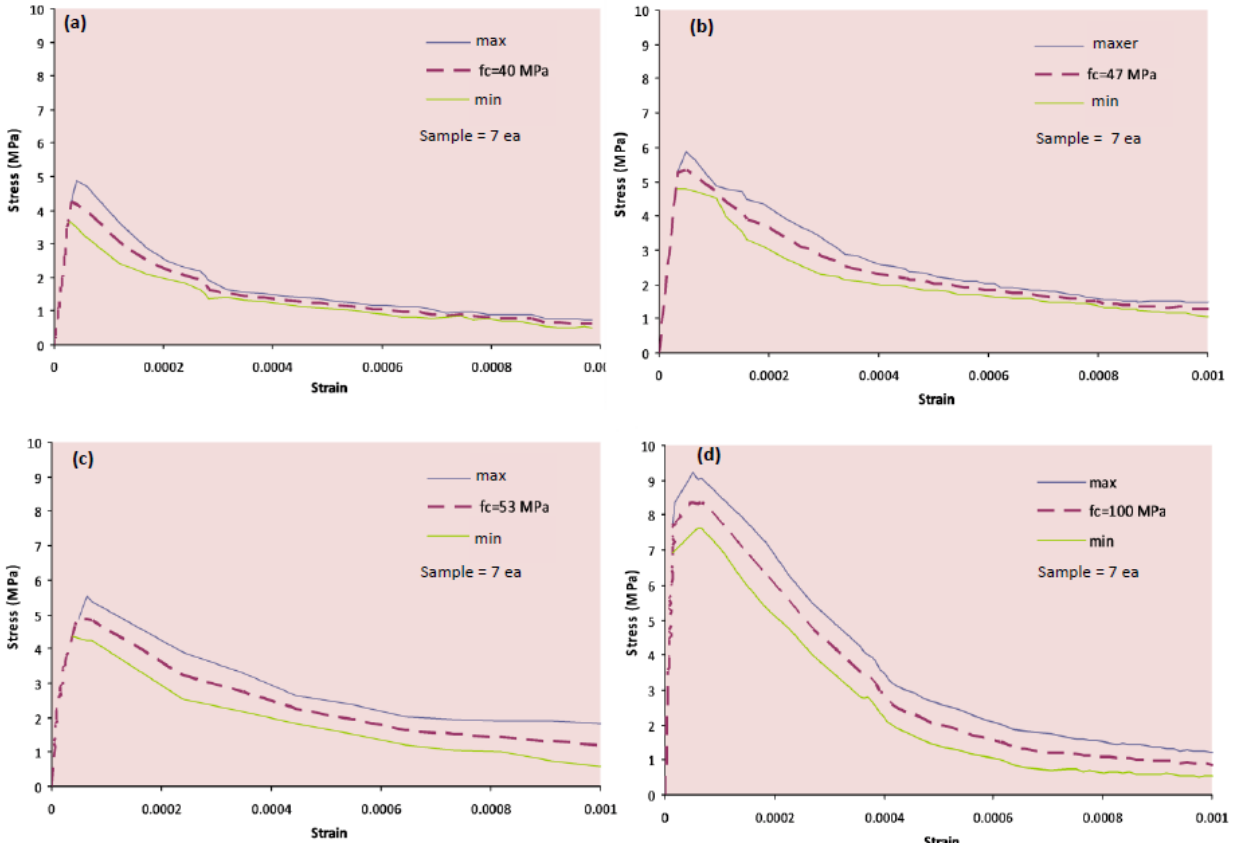

Figure 3 Variability of experimental results for compressive strength of: (a) 40 MPa; (b) 47 MPa; (c) 53 MPa; and (d) 100 MPa

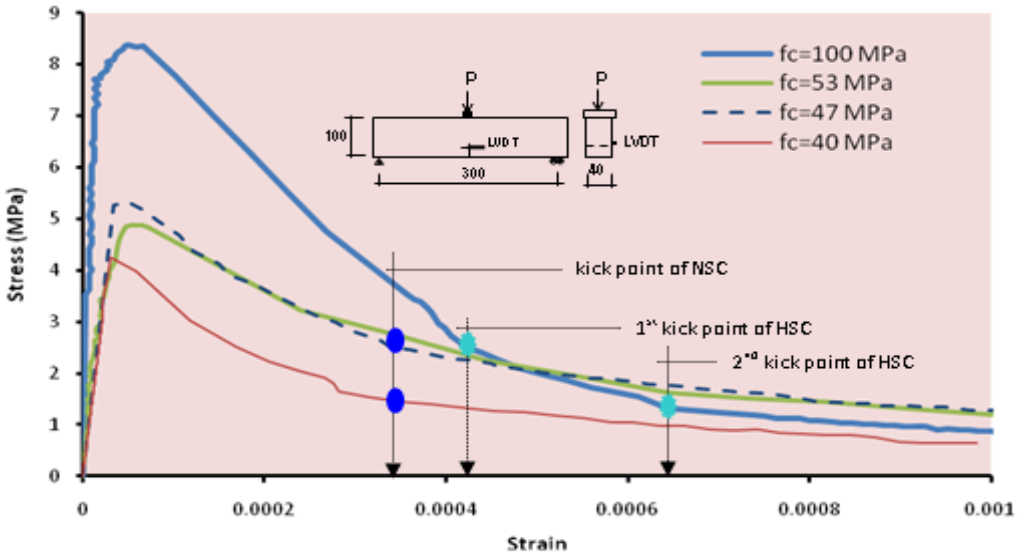

Figure 4 Stress–strain curves of various compressive strengths

The effect of increasing concrete strength on the fracture characteristics of concrete as measured by K_{IC}, G_F, and l_{ch} are shown in Figures 6, 7, and 8. K_{IC} is a parameter used to determine the fracture toughness of a material (Elfgren, 1989; Bazant & Giraudon, 2002; Zhu & Joyce, 2012). This parameter has been used often to examine the initial cracking of materials (Prokopski & Langier, 2000). Figure 6 illustrates how increasing the concrete strength helped increase the material's resistance to fracture. In the present study, initial cracks in the observed concrete occurred according to concrete strength: the stronger the concrete, the higher the applied load needed to create an initial crack. Reducing the porosity of the concrete, increasing the stiffness matrix and paste/aggregate interface zone by reducing the water–cement ratio, and incorporating additional cementitious materials were also observed to increase the strength of the concrete.

Figure 7 illustrates how G_F was observed to increase as the concrete's compressive strength rose. The G_F of NSC depended primarily on a free water–cement ratio, aggregate size, and the age of the concrete (Kozul & Darwin, 1997; fib Model Code for Concrete Structures, 2010). The utilisation of high strength aggregates in concrete led to an increase in GF values and changed the concrete's fracture behavior. Crack propagation leading to concrete failure was impeded by the aggregates; breaking tougher aggregates would change the crack orientation or multiplication of cracks, respectively. These mechanisms initiated higher energy dissipation and resulted in a different type of failure. The concrete's l_{ch}, which was proportional to the fracture process zone based on the hypothetical crack model, described the characteristics of failure (Hillerborg, 1976). The longer the l_{ch}, the longer the fracture process zone. Because the fracture process zone depicted the propagation of micro cracks, the longer fracture process zone required higher energy. This higher energy in micro crack propagation was visible in the longer tail stress–strain curve. Thus, longer l_{ch} reflected the ductile failure of materials, and shorter l_{ch} corresponded with brittle failures. As shown in Figure 8, increasing compressive strength reduced the characteristic length of the concrete, while increasing compressive strength reduced material ductility.

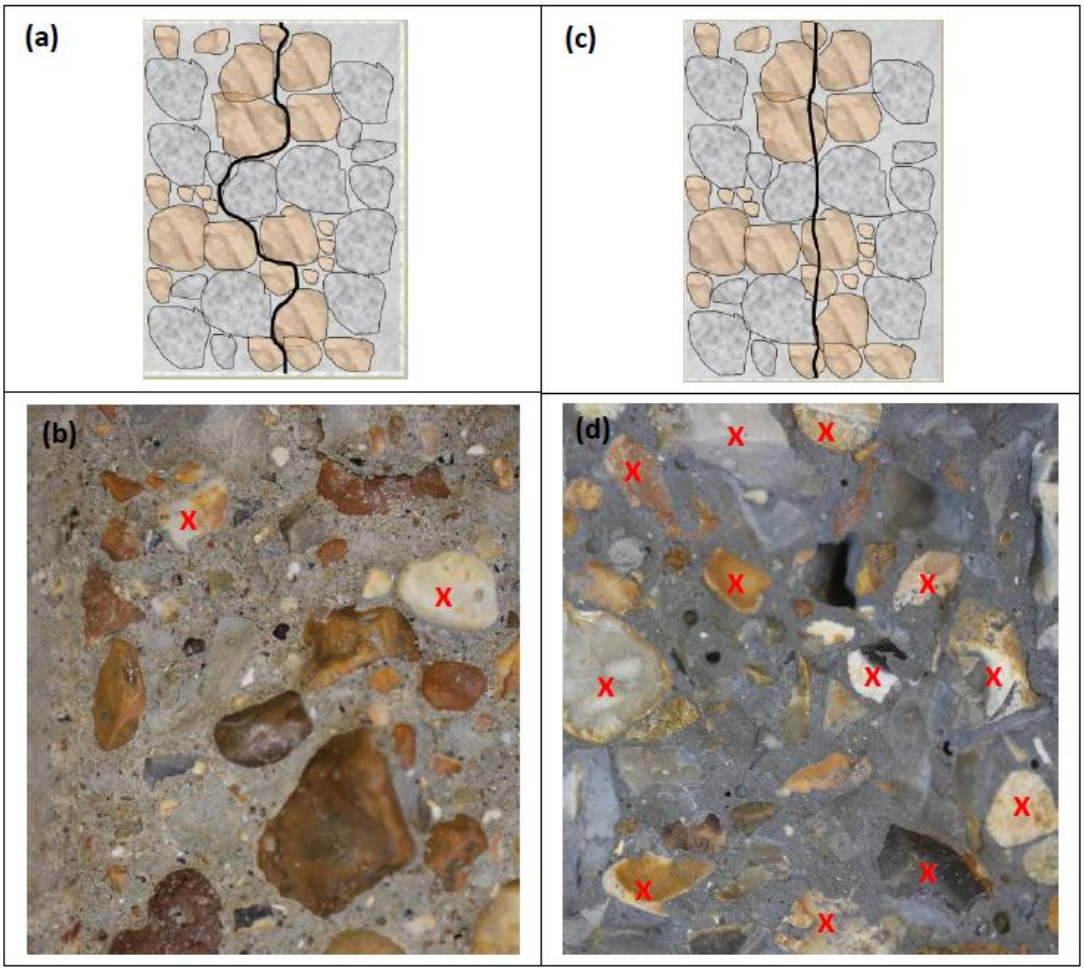

Figure 5 Typical crack growth in concrete: (a) crack propagation passes around the aggregate/cement interface; (b) surface failure of NSC; (c) crack propagation through aggregate particles; (d) surface failure of HSC (**x** is a label for aggregate fracture)

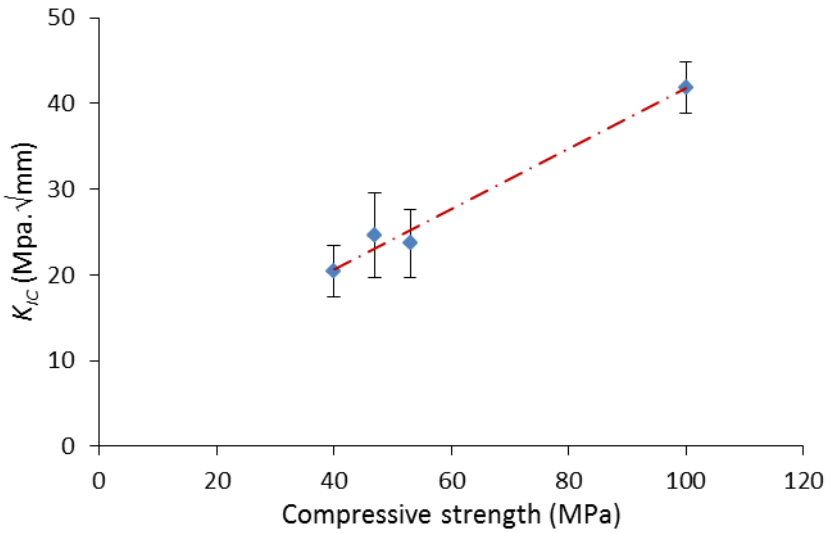

Figure 6 Effect of compressive strength on K_{IC}

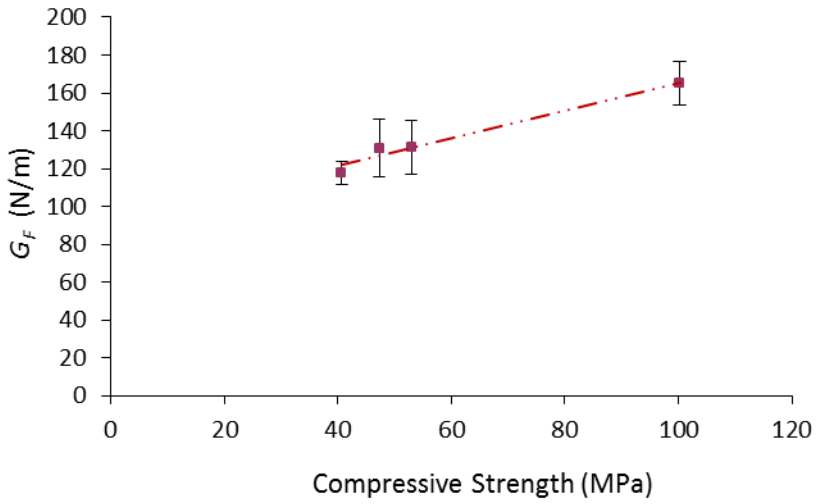

Figure 7 Effect of compressive strength on G_F

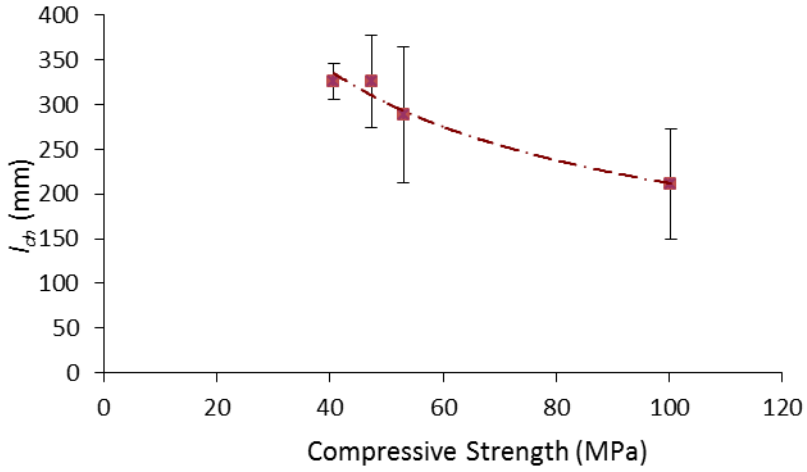

Figure 8 Effect of compressive strength on l_{ch}

5. CONCLUSION

Based on the experimental results in the present study, which investigated the effect of concrete strength on the behavior of concrete failure via a TPB test, the following conclusions have been drawn: (1) Increasing concrete strength leads to a significant increase in fracture energy value and critical stress intensity factor of the concrete, but it decreases the characteristic length of the concrete; (2) Improving the strength of the concrete increases fracture toughness but reduces ductility.

6. REFERENCES

Bazant, Z.P., Becq-Giraudon, E., 2002. Statistical Prediction of Fracture Parameters of Concrete and Implications for Choice of Testing Standard. *Cement and Concrete Research*, Volume 32, pp. 529–556

BS EN 12390-3, 2001. Testing Hardened Concrete. *European Committee for Standardization*, Brussels, Belgium

BS EN450-1, 2005. Fly Ash for Concrete: Finesses Category S. *European Committee for Standardization*. Brussels, Belgium

Elfgren, L., 1989. Fracture Mechanic of Concrete Structures: From Theory to Applications.

RILEM Report. London, UK: Chapman and Hall

Ernst, Sohn, 2010, 2013. *Fib Model Code for Concrete Structures*. Berlin, Germany

Hillerborg, A., Modeer, M., Peterson, P.E., 1976. Analysis of Crack Formation and Crack Growth by means of Fracture Mechanics and Finite Element. *Cement and Concrete Research*, Volume 6(6), pp. 773–782

Ince, R., Alyamaç, E.K., 2008. Determination of Fracture Parameters of Concrete based on Water-Cement Ratio. *Indian Journal of Engineering and Material Science*, Volume 15, pp. 14–22

Kozul, R. Darwin, D., 1997. Effects of Aggregate Type Size and Content on Concrete Strength and Fracture Energy. *Structural Engineering and Engineering Materials SM Report* No. 43. Lawrence, Kansas: University of Kansas Centre for Research Inc.

Picard, D., Leguillon, D., Putot, C., 2006. A Method to Estimate the Influence of the Notch-Root Radius on the Fracture Toughness Measurement of Ceramics. *Journal of the European Ceramic Society*, Volume 26(8), pp. 1421–1427

Prokopski, G., Langier, B., 2000. Effect of Water/Cement Ratio and Silica Fume Addition on the Fracture Toughness and Morphology of Fractured Surfaces of Gravel Concretes. *Cement and Concrete Research*, Volume 30(9), pp. 1427–1433

RILEM TC50-FCM Recommendation, 1990. Fracture Mechanic of Concrete Test Method. *Material and Structures*, Volume 23, pp. 247–252

RILEM, 1985. Determination of the Fracture Energy of Mortar and Concrete by Means of Three-point Bend Tests on Notched Beams. *Material and Structures*, Volume 18(106), pp. 285–290

Sagar, R.V., Prasad, R.V., Prasad, B.K. R., Rao, M.V.M.S., 2013. Micro Cracking and Fracture Process in Cement Mortar and Concrete: A Comparative Study using Acoustic Emission Technique. *Experimental Mechanics*, Volume 53(7), pp. 1161–1175

Scholtès, L., Donzé, F.V., 2013. A DEM Model for Soft and Hard Rocks: Role of Grain Interlocking on Strength. *Journal of the Mechanics and Physics of Solids*, Volume 61(2), pp. 352–369

Shah, S.P., Ahmad, S.H., 1994. High Performance Concrete and its Applications. London, UK: Edward Arnold Press Ltd

Shah, S.P., Swartz, S.E., Ouyang, C., 1995. *Fracture Mechanics of Concrete*. New York, USA: John Willey & Sons

Wittmann, F.H., 2002. Crack Formation and Fracture Energy of Normal and High Strength Concrete. *Sadhana Journal*, Volume 27(4), pp. 413–423

Zhu, X.K., Joyce, J.A., 2012. Review of Fracture Toughness (G, K, J, CTOD, CTOA), Testing and Standardization. *Engineering Fracture Mechanics*, Volume 85, pp. 1– 46